9th ANKARA INTERNATIONAL AEROSPACE CONFERENCE **AIAC-2017-169**
20-22 September 2017 - METU, Ankara TURKEY

UNDERSTANDING HYDRODYNAMICS OF TUNA FISH HYDROFOIL USING CFD SIMULATIONS

Abdullah Muratoglu[1*]
Batman University
Batman, Turkey

Abdurrahim Muratoglu[2]
Middle East Technical University
Ankara, Turkey

ABSTRACT

The main scope of this study is to understand the main hydrodynamic properties 2D body section of Tuna fish hydrofoil. The body coordinates were written into a 2D file which is similar to classical airfoil data files. CFD simulations of the section have been conducted by ANSYS CFX software. The hydrodynamic properties of the hydrofoil such as lift, drag and pressure coefficients were evaluated. The velocity, pressure and turbulence kinetic energy distributions have been illustrated. The analyses were made considering different angles of attack and Reynolds Number. The calculated hydrodynamic characteristics have been discussed and compared with the literature.

Keywords: Hydrofoil, Hydrodynamic, CFD, Albacore Tuna, ANSYS CFX

INTRODUCTION

The most efficient and optimum designs are found in nature. Many scientist and engineer has successfully transferred natural phenomenon to science and technology. 2D sections of airfoil and hydrofoils are employed in many areas such as turbomachinery, aircrafts and other air and marine vehicles. The blade sections have also been used by birds and fishes since thousands of years. Authors believe that, the efficiency of engineering devices could be increased and technical problems could be solved by mimicking flying and swimming animals and insects.

Albacore tuna (Thunnus Alalunga) is one of the high speed fish species. According to biological reports; its cruising speed is around 6-8 m/s with Reynolds number (Re) greater than $1x10^6$. Its burst speed can exceed 10 m/s with ten times of cruising Re (Figure 1). The main reason behind concentrating on Albacore Tuna in this study is their well streamlined body and simplicity of their body hydrofoil which can be easily obtained by excluding its fins and finlets.

The caudial, pectoral, anal, dorsal and pelvic fins together with finlets have been removed from a real scale albacore tuna fish surface (Figure 2). The images were imported to an image processing software (MATLAB) and the hydrofoil has been generated fitting 3rd degree

[1*]Assist. Prof. in Department of Civil Engineering, Email: abdullah.muratoglu@batman.edu.tr (corresponding author)
[2] GRA in Department of Aerospace Engineering, Email: moglu@metu.edu.tr

B-spline curve using 15 control points. The coordinates of the section has been normalized and digitalized. Than the hydrofoil data file has been obtained for further processing.

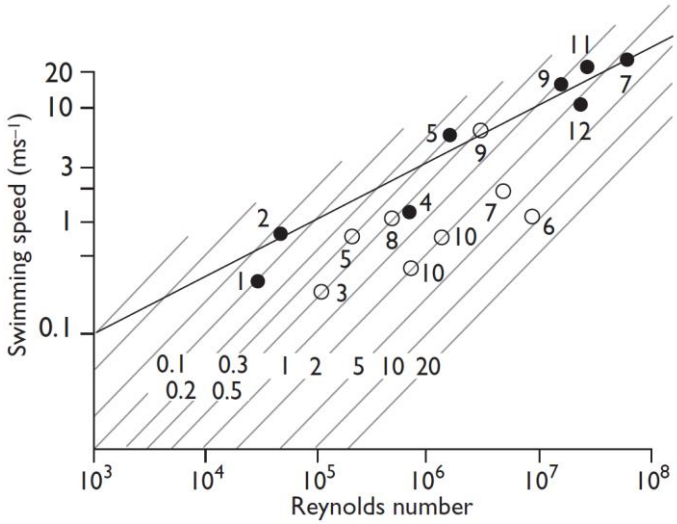

Figure 1*:* Re number vs. swimming speed of various fish species [Bone and Moore, 2008] (Open circle: Cruising speed, closed circle: Burst speed)

Figure 2: Albacore Tuna (left, image courtesy of Diane Rome Peebles at igfa.org) and the hydrofoil generated from the image (right)

Then, the hydrodynamic properties (lift, drag and pressure coefficients) of tuna fish hydrofoil have been simulated by ANSYS software. ANSYS DesignModeler and ANSYS Meshing software were used for geometry and grid generations. CFX code with Shear Stress Transport (SST) turbulence model was employed for computational fluid dynamics (CFD) simulations. Lift, drag and pressure coefficients were analyzed for Re numbers of 0.1×10^6, 1×10^6 and 10×10^6 and for various angles of attack. Velocity, pressure and turbulence kinetic energy distributions were contour plotted by the CFD-Post software for $Re=1 \times 10^6$. The simulation results were also discussed for hydrodynamic and aerodynamic point of view.

METHOD

Representation of hydrofoil by B-spline curves

Representation of the airfoil or hydrofoils using B-spline curves is a very common operation in the literature. Basically, a spline curve is defined to have a number of curve segments which are connected to form a single continuous curve like piecewise collection of Bezier curves [Sederberg, 2016]. B-spline curves are also known as NURBS (Non-uniform rational B-spline) and often used by many computer software especially CAD based and 3D modeling drawing codes [McLean, 1999]. B-spline curves are very advantageous for local adjustment of airfoil profiles especially the trailing edge. The complicated curve of the surface can be easily controlled by B-Spline theory [Wang et. al, 2013]. The airfoil chord can be

transferred to x-y coordinate system by using` B-Spline curves. High number of control points results more smooth curves whereas, small number of control points create more lively curves [Dahl and Fuglsang, 1998].

An airfoil geometry has been defined by 13 control points of Bezier curve by [Grasso, 2011]. [Dahl and Fuglsang, 1998] employed B-Spline curves with 13 control points with the degree of 5 in order to state the airfoil upper and lower surfaces before the optimization process. [Mauclere, 2009] reported that, any airfoil can be sufficiently modeled by B-Spline curves using a total number of 14 control points with degree of 4.

SST turbulence model

SST k-ω model [Menter, 1994] is a widely used two equation eddy viscosity turbulence model. The model combines both Wilcox k-ω and standard k-ε turbulence models. The accurate modelling of the viscous near-wall layers could be provided by k-ω model. The region away from the walls is suggested to be modeled by k-ε models. Using advantages of two different models makes Menter's SST method a successful and widely used approach [Muratoglu, 2014].

Both k and ω equations are given by [Versteeg and Malalasekera, 2007] as below [Muratoglu, 2014];

The *k* equation is;

$$\underbrace{\frac{\partial(\rho k)}{\partial t}}_{\substack{\text{rate of}\\ \text{change}\\ \text{of } k}} + \underbrace{div(\rho k\mathbf{U})}_{\substack{\text{transport of } k\\ \text{by convection}}} = \underbrace{div\left[\left(\mu + \frac{\mu_t}{\sigma_k}\right) grad(k)\right]}_{\text{transport of } k \text{ by turbulent diffusion}} + \underbrace{\left(2\mu S_{ij}.S_{ij} - \frac{2}{3}\rho k\frac{\partial U_i}{\partial x_j}\delta_{ij}\right)}_{\substack{\text{production}\\ \text{rate of } k}} - \underbrace{\beta_1 \rho k\omega}_{\substack{\text{dissipation}\\ \text{rate of } k}} \quad (1)$$

The omega equation is;

$$\underbrace{\frac{\partial(\rho\omega)}{\partial t}}_{\substack{\text{rate of}\\ \text{change}\\ \text{of } \omega}} + \underbrace{div(\rho\omega\mathbf{U})}_{\substack{\text{transport of } \omega\\ \text{by convection}}} = \underbrace{div\left[\left(\mu + \frac{\mu_t}{\sigma_{\omega,1}}\right) grad(\omega)\right]}_{\text{transport of } \omega \text{ by turbulent diffusion}} + \underbrace{\gamma_2\left(2\rho S_{ij}.S_{ij} - \frac{2}{3}\rho\omega\frac{\partial U_i}{\partial x_j}\delta_{ij}\right)}_{\substack{\text{production}\\ \text{rate of } \omega}} - \underbrace{\beta_2\rho\omega^2}_{\substack{\text{dissipation}\\ \text{rate of } \omega}} + \underbrace{2\frac{\rho}{\sigma_{\omega,2}\omega}\frac{\partial k}{\partial x_k}\frac{\partial \omega}{\partial x_k}}_{\text{cross diffusion term}} \quad (2)$$

Where; k is the turbulent kinetic energy (m^2/s^2), ε (epsilon) is the turbulence eddy dissipation rate (m^2/s^3), ω (omega) is the turbulence frequency ($\omega = \varepsilon/k$), $\mathbf{U}$ is the average velocity vector, μ is the fluid's viscosity, μ_t is the turbulent or eddy viscosity ($\mu_t = \rho k/\omega$), δ_{ij} is the Kronecker delta, *div* is the mathematical divergence operator, *grad* is the mathematical gradient operator, S is the deformation rate of fluid for mean flow and the cross diffusion term arises from $\varepsilon = k\omega$ transport in the epsilon equation. The model constants are; σ_k=1, $\sigma_{\omega,1}$=2, $\sigma_{\omega,2}$=1.17, γ_2=0.44, β_1=0.09 and β_2=0.083.

CFD SIMULATIONS

Geometry and grid generation

ANSYS Geometry and ANSYS Meshing tools have been used at the pre-processing stage. The solution domain has been assigned to be 20 times of the hydrofoil chord length (Figure 3) in which, the hydrofoil is at the center of the domain. C shape of domain has been used at the leading edge site for inlet boundary condition. Mapped face meshing with quadrilateral type of grid has been used. An approximate number of 90000 nodes and elements have been generated for each analysis.

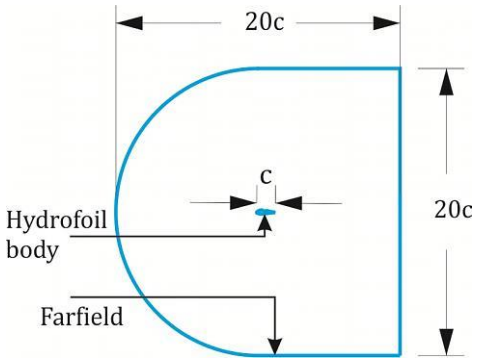

Figure 3: Illustration of the computational domain

Grid refinement

Advanced size function properties have been used in order to increase the number of cells toward to the hydrofoil wall (Figure 4). For the grid refinement, the mapped face meshing with edge sizing operation was preferred. The number of divisions from the wall to the farfield is assigned to be 150 and bias factor is selected to be 50. No inflation layer was used because of the quadrilateral type of grid.

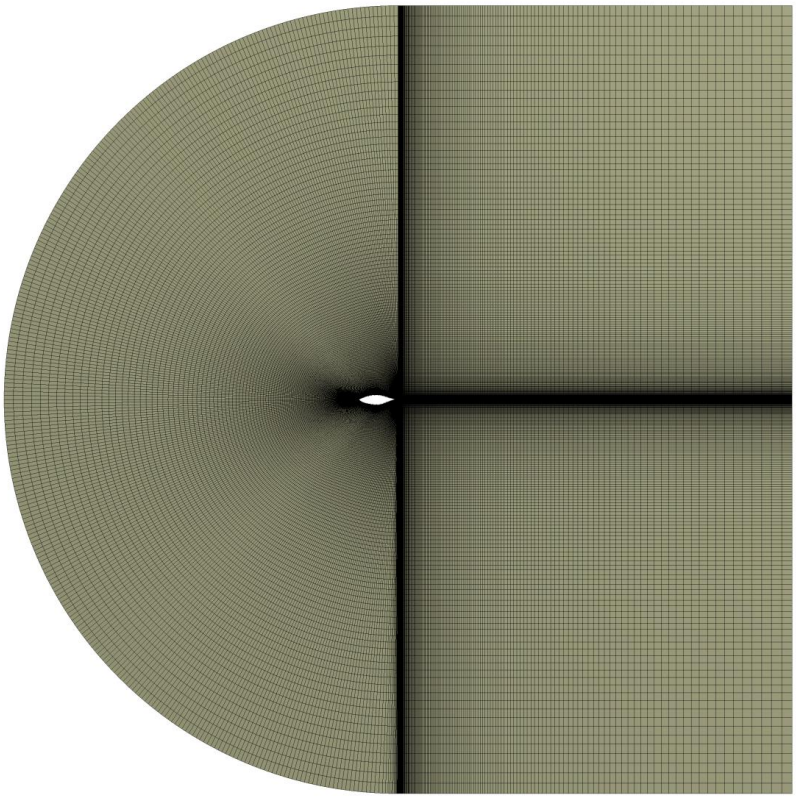

Figure 4: Quadrilateral grid around hydrofoil

The number of grids around leading edge and especially at the trailing edge site have been sufficiently refined (Figure 4).

The mesh quality metrics: The average skewness was found to be 0.007 with a maximum value of 0.4. Average aspect ratio is 4.3 with maximum value of 49. Finally, the average orthogonal quality was 0.98. The y+ values have been found to be between 0 and 300. Details about y+ value are given at Results and Discussion section.

Boundary layers and solution domain

The velocity inlet with variable speeds (for Re number modification) and pressure outlet with subsonic flow regime has been assigned. The turbulence intensity at the inlet was chosen to be medium with a value of 5 %. The hydrofoil wall was introduced to be no slip condition with smooth roughness. Finally, both sides of 2D domain were assigned to be symmetry planes (Figure 5).

The solution domain was selected to be stationary fluid domain with continuous fluid morphology. The turbulence model was assigned to be SST with automatic wall function.

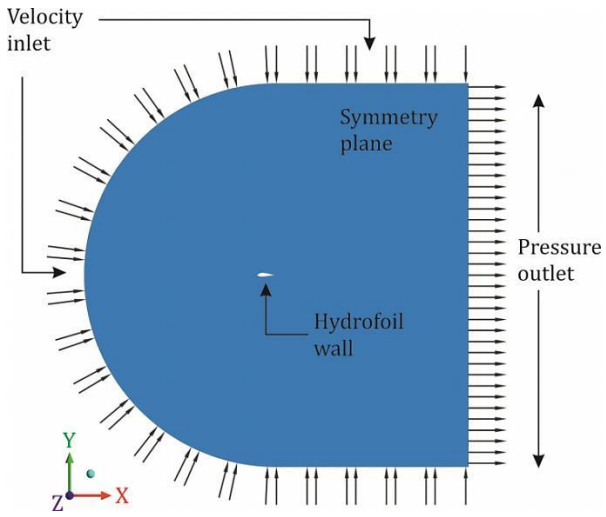

Figure 5: Boundary layers

CFD solution and convergence

The solutions have been converged with root mean square (RMS) values of pressure and momentums to be below 10^{-5}. The simulations have been conducted for various range of Re number and angle of attack. The lift and drag coefficients for different Re numbers are given in Table 1. The lift and drag coefficient distributions for various angles of attack at Re=1 million is are given in Figure 4.

RESULTS AND DISCUSSIONS

y+ value

Generally lower values of y+ are a desired requirement. For logarithmic wall functions, the first grid's centroid should be located within 30<y+<300. However, for the resolved wall treatment, the centroid of wall-adjacent grid should be within viscous sublayer which makes y+ value to be around 1. For logarithmic based wall function approach, y+ is suggested to be below 300 in order of the simulations to be valid. On the other hand, for resolved wall treatment and wall functions are not used, this value should be below 1. [ANSYS, 2011].

In this study, the y+ values were varied along the hydrofoil surface. Different y+ value configurations were obtained for different simulations with modification of Re number and angle of attack. However, the y+ values for all cases were between 0 and 300. According to the software sources, this value is not ideal but it is acceptable because of used turbulence model type and utilization of wall function. On the other hand, all the reported solutions are converged with the residuals below 10^{-5} (RMS values of pressure and momentums) which shows the accuracy of the simulations. Consequently, the authors state that, the y+ values should be improved for future studies.

Lift and drag characteristics

Distribution of lift and drag coefficients of Tuna fish hydrofoil at Re=1 million is given in Figure 6. The lift coefficient at zero angle of attack is around 0.012 which shows the hydrofoil has a nearly symmetrical shape with a very low chamber value. The relationship between lift coefficient and angle of attack varies linearly until the stall angle, which is a characteristic property of artificial designed airfoils.

On the other hand, a smooth behavior around the stall angle is observed in which there is no a sudden drop in the lift coefficient. Therefore, the value of $C_{l,max}$ is almost steady around the angles of attack between 10°-16°. The stall angle is determined to be 13°. This section could be employed at stall regulated turbines in which minimal variation is desired around the stall angle. Utilizing the section in pitch regulated turbines is not suggested due to this property. The drag characteristic of the section is said to be reasonable comparing with NACA sections having similar geometry.

The lift and drag coefficients at 10° angle of attack and at various Re number is given in Table 1. The same mesh was employed at these CFD simulations. This only gives preliminary and rough idea about the variation of lift and drag characteristics at different Re numbers. For detailed and more accurate approach, the grid should be well improved especially at low Re numbers.

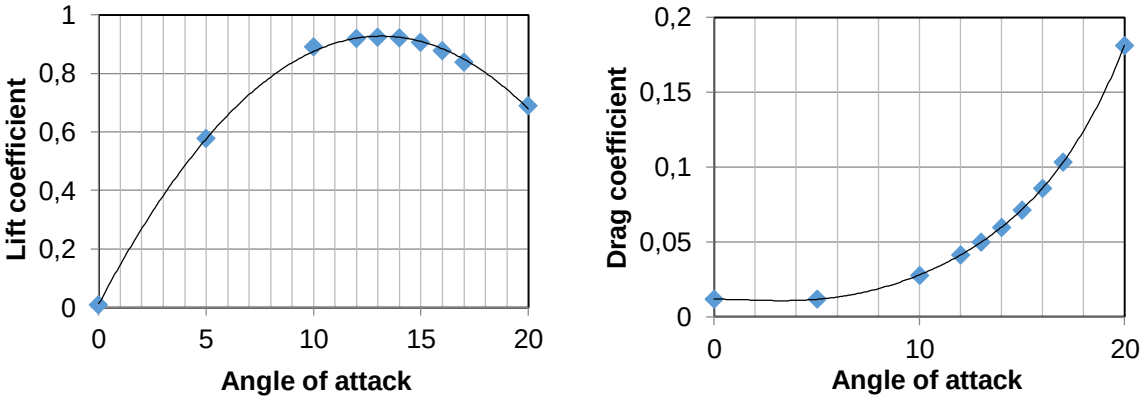

Figure 6: Lift and drag coefficient distribution at Re=1 million

Table 1: Lift and drag coefficients of tuna fish hydrofoil at different Reynolds number (α=10°)

Re	C_l	C_d
50,000	0.54	0.05
100,000	0.69	0.04
1,000,000	0.89	0.03
10,000,000	0.94	0.02

Pressure coefficient

In the case of utilizing the hydrofoil in hydrokinetic turbines or ship propellers, the pressure coefficient should be well studied for cavitation point of view. The pressure coefficient graphs vs. percent (normalized) chord were illustrated in Figure 7. It can be said that, the section has relatively reasonable pressure coefficient distribution at various Re numbers and angles of attack. The RISO-A family of airfoil with the similar thickness has lower pressure coefficient values over various conditions. However, the pressure characteristics of tuna fish section are very similar to NACA 63-818 section which is a widely used profile in hydrokinetic turbines. For detailed information and utilization, the device or technology based specifications should be analyzed.

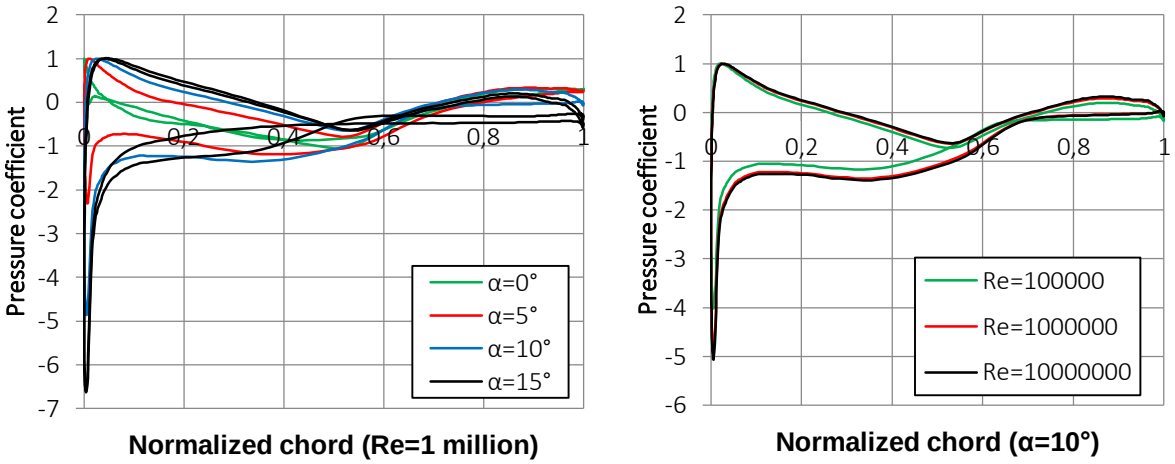

Figure 7. Pressure coefficient distributions for various angles of attack and Re number

Visualizations of the flow field

The illustrations of velocity, pressure and turbulence kinetic energy at the flow area (Re=1 million and α=0°,5°,10°,15°) are given in Figures 8-10. A special emphasise should be made on flow separation over the upper surface of the hydrofoil. Both velocity and turbulence kinetic energy contour plots shows that the flow separation develops at the rear region of the section which is close to the trailing edge. This situation is a desired phonemenon and it can be verified by lift characteristic of the profile.

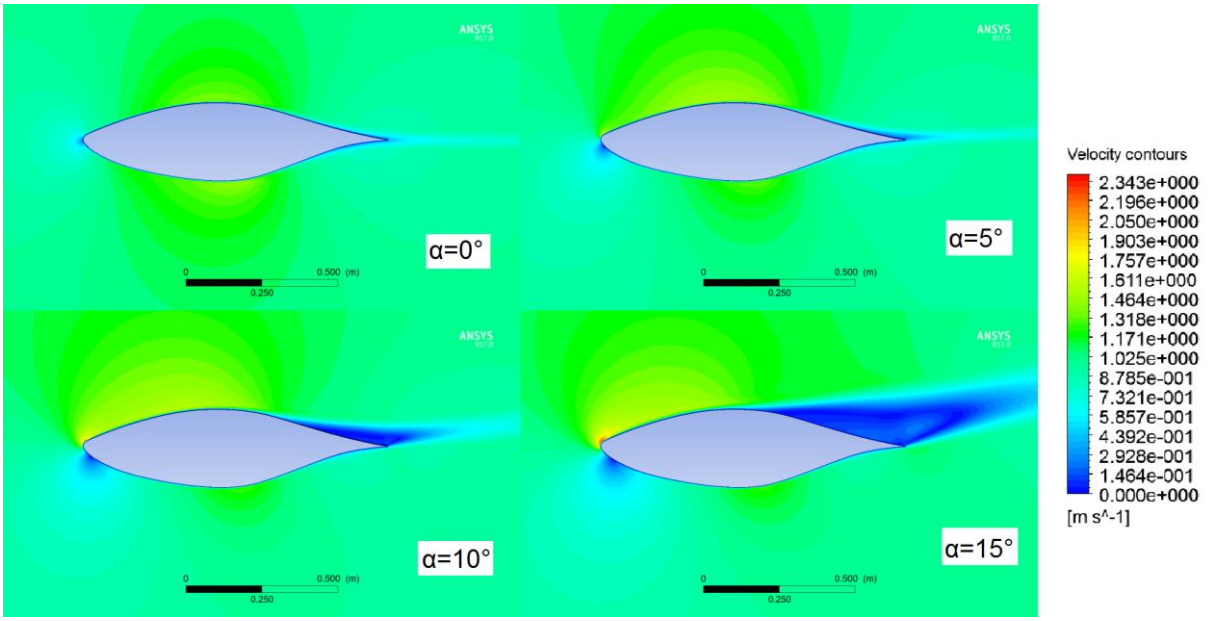

Figure 8. Velocity distributions around hydrofoil at Re=1 million

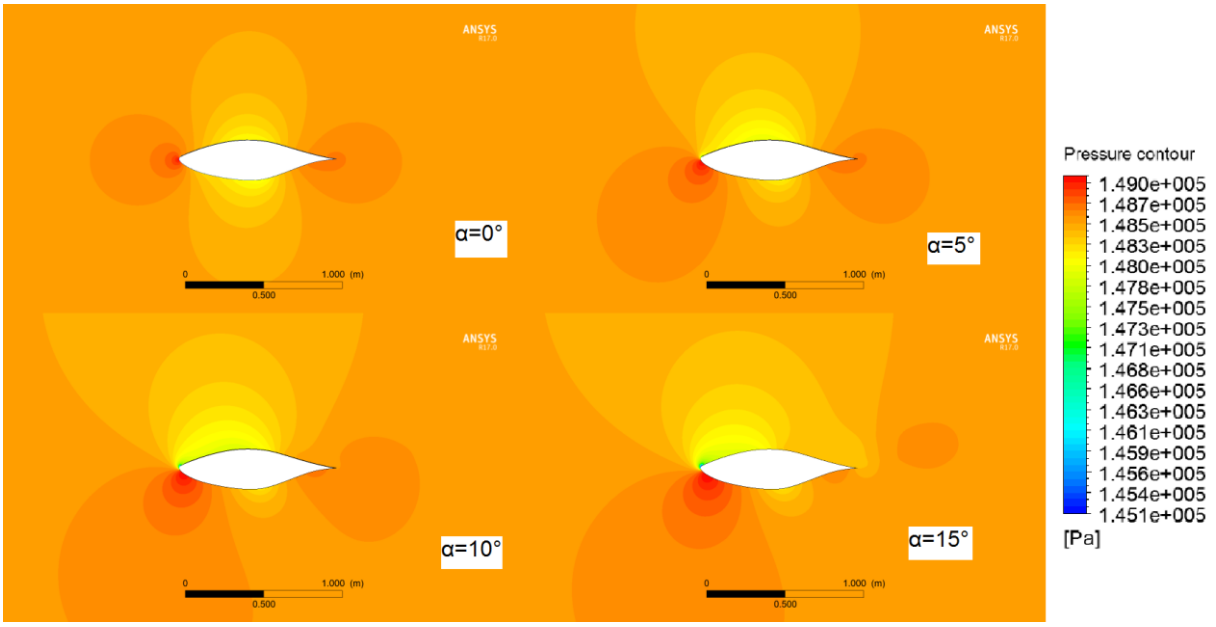

Figure 9: Pressure distributions around the hydrofoil at Re=1 million

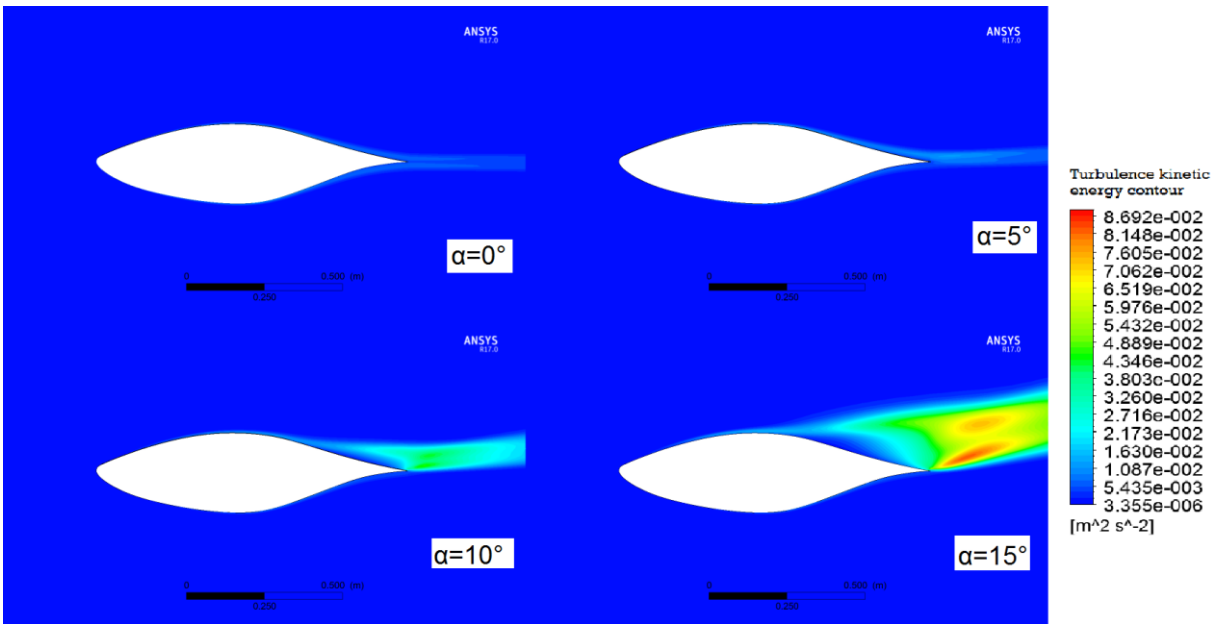

Figure 10: Turbulence kinetic energy distributions around the hydrofoil at Re=1 million

CONCLUSION

A hydrofoil was generated from the Albacore Tuna fish body (Thunnus Alalunga) and it has been digitalized by curve fitting employing widely used B-spline method. Then, the hydrodynamic performance has been evaluated by CFD analyses using SST k-ω turbulence model. The performance outputs have been interpreted considering lift, drag, pressure coefficient distributions and visualization of the post-processing results. The section exhibits good performance for stall regulated turbines with a smooth stall characteristic. Having relatively lower pressure coefficient distribution is a desired feature for water environment. Finally, the situation of the flow separation which is found to be close to the trailing edge can be expressed as a good performance criterion. Consequently, Thunnus Alalunga has a hydrofoil shape which is optimized for its environment. Making required modifications, this naturally optimized section could be adapted to turbine technology.

References

ANSYS (2011) *Introduction to ANSYS CFX, Lecture notes on Turbulence*, ANSYS Inc.

Bone, Q. and Moore, R.H. (2008) *Biology of Fishes*, Taylor and Francis, e-book.

Dahl, K.S and Fuglsang P. (1998) *Design of the wind turbine airfoil family* RISØ-A-XX, Risø National Laboratory, Roskilde, Denmark.

Grasso F. (2011) *Design and optimization of tidal turbine airfoil,* 29th AIAA Applied Aerodynamics Conference, 27-30 June 2011, Honolulu, HI, USA.

Mauclere, X. (2009) *Automatic 2D airfoil generation, evaluation and optimization using MATLAB and XFOIL,* M.Sc. dissertation at Mechanical Engineering Department of Technical University of Denmark.

McLean, M. (1999) *A windows program for airfoil design using B-splines*, M.Sc. thesis submitted to Rochester Institute of Technology.

Menter, F.R. (1994) *Two-Equation Eddy-Viscosity turbulence models for engineering applications,* AIAA Journal, Vol. 32(8), p: 1598-1605.

Muratoglu, A. (2014) *Design and simulation of a riverine hydrokinetic turbine*, Ph.D. Dissertation in Gaziantep University, Turkey.

Sederberg, T.W. (2016) *Computer aided geometric design course notes*, Available at: http://tom.cs.byu.edu/~557/text/cagd.pdf

Versteeg H. K. and Malalasekera W. (2007) *An introduction to computational fluid dynamics, the finite volume method,* Pearson, 2nd edition.

Wang, Q., Chen, J., Pang, X., Li, S., Guo, X. (2013) *A new direct design method for the medium thickness wind turbine airfoil*, Journal of Fluids and Structures, Vol. 43, p:287-301.

Answer to reviewers:

Details of the grid refinement have been written in the manuscript.

Details of y+ values and a discussion is provided.

Using the same mesh at various Re numbers is not suitable for detailed analyses of the sections. However, in this study, the drag and lift coefficients at 10° of angle of attack at various Re numbers are provided in order to provide a rough and preliminary idea about the Re number dependency of the hydrofoil. We discussed this point.

The Re number at some figures were accidentally forgotten. Required corrections have been applied.